Preparation and Properties of Floral CaO/ZnO Nanocomposite From Achatina Fulica Snail Shell

Qiushi Jiang
Jilin Agricultural University
Zhaolian Han
Jilin Agricultural University
Yafeng Yuan
Jilin Agricultural University
Zhiqiang Cheng (czq5974@163.com)
Jilin Agricultural University https://orcid.org/0000-0003-1156-0540

Research Article

Keywords: ZnO, Achatina fulica, sustainable material, photocatalyst, microstructure, rhodamine B

Posted Date: June 23rd, 2021

DOI: https://doi.org/10.21203/rs.3.rs-592177/v1

Abstract

In this study, CaO prepared by calcination treatment from abandoned *Achatina fulica* shell was used as a raw material, and the nano-flower-like CaO/ZnO photocatalytic composite material was prepared through co-precipitation method. SEM study showed ZnO with spindle-like petals in the range of 500-1000 nm grown on the surface of CaO carrier. The mapping image shows that the base component of the nanometer flower is mainly CaO, which is because CaO is not only in the reaction as a carrier, but also creates an alkaline environment in the methanol system, which is advantageous for co-precipitation. UV-vis spectroscopy shows that the visible light absorption of composites has red shifts, besides, PL, EIS and photocurrent test showed that the composites have stronger electronic hole separation capabilities. The visible light degradation test of rhodamine B showed that CaO/ZnO photocatalytic composite could degrade 90% of the pollutants in 25 min, superior to CaO and ZnO, exhibiting recyclability properties, which is a potential candidate with cost-effective and sustainable photocatalysts.

1. Introduction

Achatina fulica is a strong field pest, which can be as long as 20 cm. It is now used in food sources and livestock farming. However, the snail shell has become a waste in the environment, which has caused a threat to production and daily life of human beings(Puspitasari et al. 2021). The snail shell has a rich amount of Ca element, and has a unique microstructure, as an alternative source of CaO. Moreover, rational utilization of shell resources to construct photocatalysts can not only reduce the production cost, but also be used for pollution control, which has good ecological and economic benefits(Roschat et al. 2016; Laskar et al. 2018; Pooladi and Bazargan-Lari 2020).

Metal oxide Semiconductors are the primary choice of photocatalysts. ZnO has high visible light response, high efficiency and low cost, which is suitable for industrial applications(Peter et al. 2020). However, due to low activity area and photocorrosion, its effect is inhibited in practical applications(Promdet et al. 2019). A large number of studies have been conducted to enhance the performance of ZnO, in which ZnO that have different forms of different forms have been confirmed by constructing bases and co-precipitation methods have been proven to be effective preparation methods(Pan et al. 2015; Pastor et al. 2019; Guo et al. 2019).

We conducted this study to prepare a floral CaO/ZnO nanocomposite by co-precipitation from a discarded *Achatina fulica* snail shell through green ultrasonic assisted soaking and calcination method. It has the pore structure of CaO and the light response of ZnO. The visible light degradation ability of rhodamine B (RhB) by the composite is studied, and the recycling performance is studied to avoid secondary pollution.

2. Experimental

2.1 Collection and pre-processing of shells

The discarded *Achatina fulica* snail shell was collected from the market in Jilin, China, washed off the dust on the surface with water, soaked in an aqueous solution for 12 h, kept heated in boiling water for 1 h, and 10 wt.% soap solution is added for cleaning in 0.5-h ultrasonic. The shell was then rinsed with a large amount of distilled water, and kept in an oven at 105 ℃ drying to constant weight.

2.2 Preparation of CaO/ZnO composites

The shell was oxidized by high temperature air in a muffle furnace. The pretreated shell was heated to 800 ℃ at a rate of 3 ℃/min and kept for 1 h to obtain white shell CaO. After grinding, the shell was passed through a 100-mesh screen for the preparation of composite materials. 0.1 g of crushed shell CaO was taken, 6.6 mL of H_2O and 0.5 mL of methanol were added to prepare a mixed solution, then 0.5 g of $ZnCl_2$ was added, and ultrasonic treatment was conducted for 30 min. After 3 times of H_2O washing and centrifugation at 4000 rpm for 5 min, the sample was dried in a 60 ℃ oven to a constant weight, and then heated to 500 ℃ at 3 ℃/min in a muffle furnace and held 2 h to obtain light blue colored CaO/ZnO composite (Fig. 1). As a contrast, a separate ZnO crystal was prepared, the amount of material is identical to that of the CaO/ZnO composites, except that shell CaO is not added, hereinafter referred to as ZnO.

2.3 Characterization

The surface morphology of the samples was observed using a scanning electron microscope (SSX-550, Shimadzu), and the elemental composition of the samples was analyzed using an energy dispersive X-ray spectrometer (SEDX-500, Shimadzu). TEM (Fei Tecnai G2) was used to observe the microstructure. An X-ray diffractometer (XRD-7000, Shimadzu) was used to determine the crystal structure of the sample. Fourier transform infrared spectroscopy (IRAffinity-1S, Shimadzu) was used to obtain the Fourier infrared spectra of the microstructure. The specific surface area and pore diameter of the samples were analyzed using the Beishide Instrument 3H-2000PS1 combined with the multipoint Brunauer-Emmett-Teller (BET) and Barrett-Joyner-Halenda (BJH) methods. The light absorption characteristics of the samples and the degradation of the dyes were studied by UV-Vis spectrophotometer with integrating sphere (TU-1950, Beijing Purkyne Corporation). The light responsiveness of the sample was analyzed using a fluorescence spectrophotometer (F-4500, HITACHI). The photocurrent response and electrochemical impedance spectra of the catalyst were analyzed by electrochemical workstation (CHI760E, Chenhua, Shanghai).

2.4 Photocatalytic ability test

The photocatalytic properties when RhB was as an analog contaminant test sample were tested in Shanghai Bron's BL-GHX eight-position Photoreactor, using a high-pressure mercury lamp with visible light filter as the light source. 10 mg of catalyst was dispersed in a 30 mL solution containing 10 $mg{\cdot}L^{-1}$ RhB and stirred under dark conditions for 90 min to achieve adsorption-desorption balance. Then the mercury lamp (360 W) was then turned on to begin the degradation experiment. The absorbance value of the mixture at 554 nm was measured by taking 3 mL out of the mixture through the filter every 5 min. Each test was repeated three times to obtain the average concentration, so as to determine the

degradation degree of RhB in the catalytic system. After each photocatalytic reaction was completed, the catalyst was separated from the reaction system by 4000 rpm by centrifugation of 5 min, rinsed with a large amount of distilled water and dried to constant weight. The above steps were repeated to test the repeatability.

In order to analyze the charge transfer mechanism of RhB under visible light degradation, free radical scavenging experiments were carried out. The effects of hydroxyl radical (·OH) and hole (h^+) on photodegradation reaction were studied using IPA and EDTA-2Na. The free radical cleavage agent was added to the reaction system at a concentration of 1 mM, and the remaining experimental conditions were the same as the photocatalytic experiment above.

3. Results And Discussion

Figure 2 shows the micromorphology of the products in each stage of the preparation process. The uncalcined snail shell (Fig. 2a) has a large number of parallel columnar crystal structures of calcium carbonate on its surface. However, the organic matter in the snail shell is oxidized at high temperature, and the calcium carbonate skeleton is decomposed into CaO, forming a uniformly distributed pore structure (Fig. 2b), which is constant and has good dispersibility. Figure 2 (c) shows the nanoflowers with spindle-like petals in the length range of 500–1000 nm, which grow on the surface of spherical CaO with different scales as the support. In the case where there is no CaO carrier, ZnO only showed rod-like agglomerated nanoparticles of 50-1000 nm (Fig. 2d). In Fig. 2(e), TEM of nanoflower confirmed the adhesion of ZnO on the surface of CaO base. Figure 2(f) shows the long-range ordered mesoporous network corresponding to ZnO (the internal spacing as 0.25 nm, corresponding to the (101) crystal plane of ZnO), while the lattice fringe of CaO is not seen, which may be because the introduction of ZnO leads to partial blockage of the carrier pores. The mapping image (Fig. 2g-j) showed that ZnO was the main spindle-like component on the surface of the nano-flower, while CaO was the main component in the nano-flower base. This structure should be because CaO not only acts as a carrier in the reaction, but also creates an alkaline environment in the methanol system, which is conducive to co-precipitation and promotes the growth of ZnO petals.

In Fig. 3 (a), the distribution of elements on the surface of shell and nano-flower was analyzed by EDX scan, and it can be seen that the calcined snail shell is pure CaO. By comparison, the surface of the CaO/ZnO photocatalyst has a large amount of Zn, uniformly distributed O and Ca components, and the method used in this study did not add impurities to the CaO/ZnO structure. The N_2 adsorption-desorption isotherms and pore size distribution of shell CaO and CaO/ZnO nanoflowers are shown in Fig. 3 (b). The adsorption-desorption isotherms of shell CaO support and CaO/ZnO are type IV curves of mesoporous materials, but the hysteric loop of CaO/ZnO is shifted to a relatively high pressure, corresponding to a larger hole increase, which may be caused by the accumulation and growth of ZnO in shell CaO to form new channels. And the specific surfaces of the shell CaO and CaO/ZnO are 17.15 m^2/g and 20.47 m^2/g, that is, the specific surface area of the composite is 1.2 times that of the shell CaO. The pore size distribution curve shows that the pore size range of CaO/ZnO is mainly in the range of 2–4 nm, similar to

that of shell CaO. Figure 3 (a) shows the FT-IR peak of the products, in which the characteristic peak distribution of the snail shell and the $CaCO_3$ material is basically consistent, and there is a significant feature peak at 705 cm^{-1}, 867 cm^{-1} and 1800 cm^{-1}, which respectively correspond to the O-C-O out-of-plane bending vibration, in-plane bending vibration and C-O stretching vibration peaks of CO_3^{2-} group. The weak peaks at 3636 cm^{-1} observed in shell CaO may be attributed to the vibration of the N-H and O-H functional groups in the structure. The wide peaks at 1450 cm^{-1} wavelength can be attributed to the O-C-O asymmetric tensile vibration peak in the CaO structure, indicating that there may be a large number of active groups on the surface of the shell CaO. Further, the O-C-O asymmetrical tensile vibration peak of shell CaO structure and the stretching vibration peak of Zn-O-Zn corresponding to ZnO at 871 cm^{-1} exist in CaO/ZnO composites. In addition, the wide peak at 3640 cm^{-1} corresponds to the hydroxyl group(Tissera et al. 2018). Figure 3 (d) shows the pattern of the shell, 2θ = 29.4°, 36.2°, 39.4°, 43.2°, 47.6°, 56.7°, 60.7°, 64.8° have a diffraction peak, corresponding to (104), (110), (113), (202), (116), (122), (214) and (300) crystal face of the calcite $CaCO_3$ (JCPDS 83–0578 Standard Card). The calcined shell corresponds to (111), (200), (200), (202) and (311) crystal plane feature (JCPDS 77-9574 Standard Card) at 2θ = 32.0°, 37.5°, 54.0°, and 64.3°. CaO/ZnO only showed a weak peak of ZnO at 36.3°, corresponding to (101) crystal plane of ZnO (JCPDS 36-1451 Standard card), consistent with HRTEM.

The ZnO itself has visible light absorption characteristics, depending on the UV-vis absorption spectrum (Fig. 4a), and the CaO/ZnO composite also has visible light absorption properties, and the absorption boundary is slightly redshifted to 416 nm. The results show that CaO/ZnO composites require less excitation energy than ZnO. In order to evaluate the charge trapping ability and the lifetime of light-induced electron-hole pairs in the semiconductor composites, the photonuminescence spectrum of ZnO nanoparticles, shell CaO and CaO/ZnO composites (Fig. 4b) are analyzed. They all have three main emission peaks. Among them, of which the peaks at 486 nm, 487 nm and 478 nm, corresponding to their near-band gap emission, while the other two weak emission peaks distributed within the 445–510 nm may be related to the oxygen vacancy formed during the reaction. The shell CaO has the highest fluorescence intensity, which means the highest optical electron-hole composite. The fluorescence intensity of the CaO/ZnO composite is lower than that of the shell CaO, indicating that the recombination of photogenerated electrons and holes can be effectively inhibited. Therefore, the reduction of charge carrier recombination rate leads to the existence of a large number of electrons and photogenerated holes at the interface of photocatalytic reaction, which promotes the photocatalytic reaction.

The photoelectric response performance of the CaO/ZnO sample was studied. As shown in Fig. 4 (a), the CaO/ZnO nanocomposite has a greater current response than ZnO under the same voltage, and the photocurrent density generated by CaO/ZnO nanocomposite is about 4.5 $mA{\cdot}cm^{-2}$, which is 1.2 times that of produced ZnO (3.8 $mA{\cdot}cm^{-2}$) and 1.9 times that of shell CaO (2.4 $mA{\cdot}cm^{-2}$). That means CaO/ZnO composite has a stronger ability to produce charge, and with the change of time, the photocurrent intensity of CaO/ZnO composites is almost unchanged, which proves that the composites have good stability. In Fig. 4 (b), electrochemical alternating current impedance (EIS) shows electronic transfer efficiency within the sample under test, in which CaO/ZnO has the smallest arc radius, indicating

that the photogenerated charge carriers within the sample are generated at a fast rate, the impedance of electrons moving within the sample is small, and the electron transfer rate is high.

Figure 6 (a) shows the degradation of RhB by different catalysts under visible light conditions. For ZnO and shell CaO, only 55% and 39% RhB after 25-min visible light irradiation. ZnO nanoparticles have a catalytic effect on RhB, but the photocatalytic efficiency is low because they are not well dispersed. However, the composite material shows a good degradation effect of 91%, which may be due to the growth of ZnO on CaO template resulting in more active sites, showing a higher apparent catalytic rate. As can be seen from Fig. 6 (b), the degradation efficiency of the sample decreased slightly after recycling, from 86% degradation within 15 min of the first time to 83%, 82%, 82% and 81% in turn. Besides, after four photocatalytic circulation, the XRD lines of CaO/ZnO are completely consistent with those shown in Fig. 3 (d), which confirmed the structural integrity. The results show that CaO/ZnO composite photocatalyst has good stability and reusability. In order to determine the main active species in the degradation process of RhB by composite photocatalyst, a variety of active species capture agents were used to carry out capture experiments (Fig. 6c). With the addition of EDTA-2Na and IPA, the degradation rates of RhB were reduced to 54% and 67%, respectively. It shows that the contribution of e^- to the reaction is stronger than that of ·OH in the photocatalytic reaction of CaO/ZnO.

4. Conclusions

The ZnO nanoflowers are uniformly formed on the surface and inside of CaO in methanol solution by a common co-precipitation method, and the obtained CaO/ZnO has a strong visible light absorption and efficient photoelectric response. Compared with the degradation effect of RhB by CaO and ZnO, the CaO/ZnO composite showed the best degradation effect within 25 min. In addition, it showed good circulating stability, indicating that CaO/ZnO nanoflowers has a wide application value in photocatalytic degradation of pollutants in water. This study provides a new idea for snail shell waste treatment and biomass composites manufacturing with enhanced performance.

Declarations

Ethics approval and consent to participate

Not applicable.

Consent to Publish

All data generated or analyzed during this study are included in this article.

Author contribution

Qiushi Jiang: Writing - original draft preparation, Investigation, Validation. Zhaolian Han: Conceptualization, Methodology, Investigation, Formal analysis. Yafeng Yuan: Investigation,

Conceptualization, Methodology. Zhiqiang Cheng: Project administration, Writing – Reviewing and Editing, Funding acquisition.

Funding information

This work was funded by Jilin Province Innovation Capacity Building Fund Project (2020C024-5), Jilin Province Science and Technology Development Project (20200708107YY) and National Key Research and Development Program of China (2019YFC0409102-2).

Competing Interests

The authors declare that they have no conflict of interest.

Availability of data and materials

Not applicable.

References

Guo T, Xu G, Tan S, et al (2019) Controllable synthesis of ZnO with different morphologies and their morphology-dependent infrared emissivity in high temperature conditions. J Alloys Compd 804:503–510. https://doi.org/10.1016/j.jallcom.2019.07.011

Laskar IB, Rajkumari K, Gupta R, et al (2018) Waste snail shell derived heterogeneous catalyst for biodiesel production by the transesterification of soybean oil. RSC Adv 8:20131–20142. https://doi.org/10.1039/C8RA02397B

Pan L, Shen G-Q, Zhang J-W, et al (2015) TiO2–ZnO Composite Sphere Decorated with ZnO Clusters for Effective Charge Isolation in Photocatalysis. Ind Eng Chem Res 54:7226–7232. https://doi.org/10.1021/acs.iecr.5b01471

Pastor A, Balbuena J, Cruz-Yusta M, et al (2019) ZnO on rice husk: A sustainable photocatalyst for urban air purification. Chem Eng J 368:659–667. https://doi.org/10.1016/j.cej.2019.03.012

Peter R, Salamon K, Omerzu A, et al (2020) Role of Hydrogen-Related Defects in Photocatalytic Activity of ZnO Films Grown by Atomic Layer Deposition. J Phys Chem C 124:8861–8868. https://doi.org/10.1021/acs.jpcc.0c01519

Pooladi A, Bazargan-Lari R (2020) Simultaneous removal of copper and zinc ions by Chitosan/Hydroxyapatite/nano-Magnetite composite. J Mater Res Technol 9:14841–14852. https://doi.org/10.1016/j.jmrt.2020.10.057

Promdet P, Quesada-Cabrera R, Sathasivam S, et al (2019) High Defect Nanoscale ZnO Films with Polar Facets for Enhanced Photocatalytic Performance. ACS Appl Nano Mater 2:2881–2889.

https://doi.org/10.1021/acsanm.9b00326

Puspitasari P, Fauzi AF, Susanto H, et al (2021) Phase identification and morphology of CaCO3/CaO from Achatina Fulica snail shell as the base material for Hydroxyapatite. IOP Conf Ser Mater Sci Eng 1034:012128. https://doi.org/10.1088/1757-899X/1034/1/012128

Roschat W, Siritanon T, Kaewpuang T, et al (2016) Economical and green biodiesel production process using river snail shells-derived heterogeneous catalyst and co-solvent method. Bioresour Technol 209:343–350. https://doi.org/10.1016/j.biortech.2016.03.038

Tissera ND, Wijesena RN, Sandaruwan CS, et al (2018) Photocatalytic activity of ZnO nanoparticle encapsulated poly(acrylonitrile) nanofibers. Mater Chem Phys 204:195–206. https://doi.org/10.1016/j.matchemphys.2017.10.035

Figures

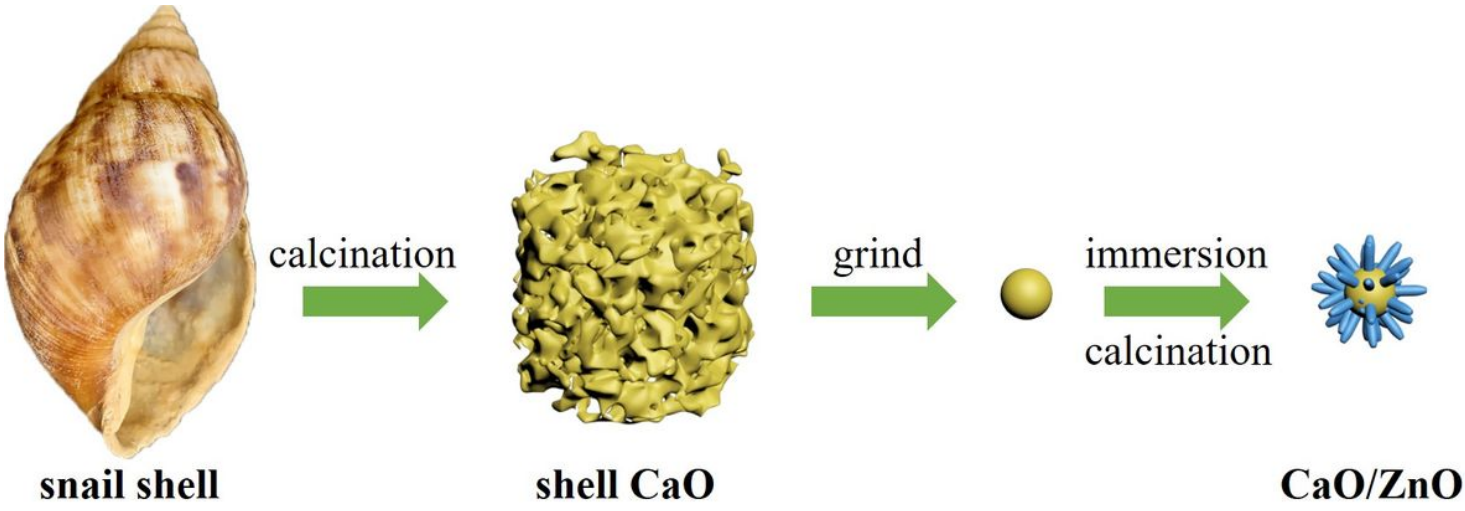

Figure 1

Schematic illustration of proposed formation processes of the as-prepared CaO/ZnO

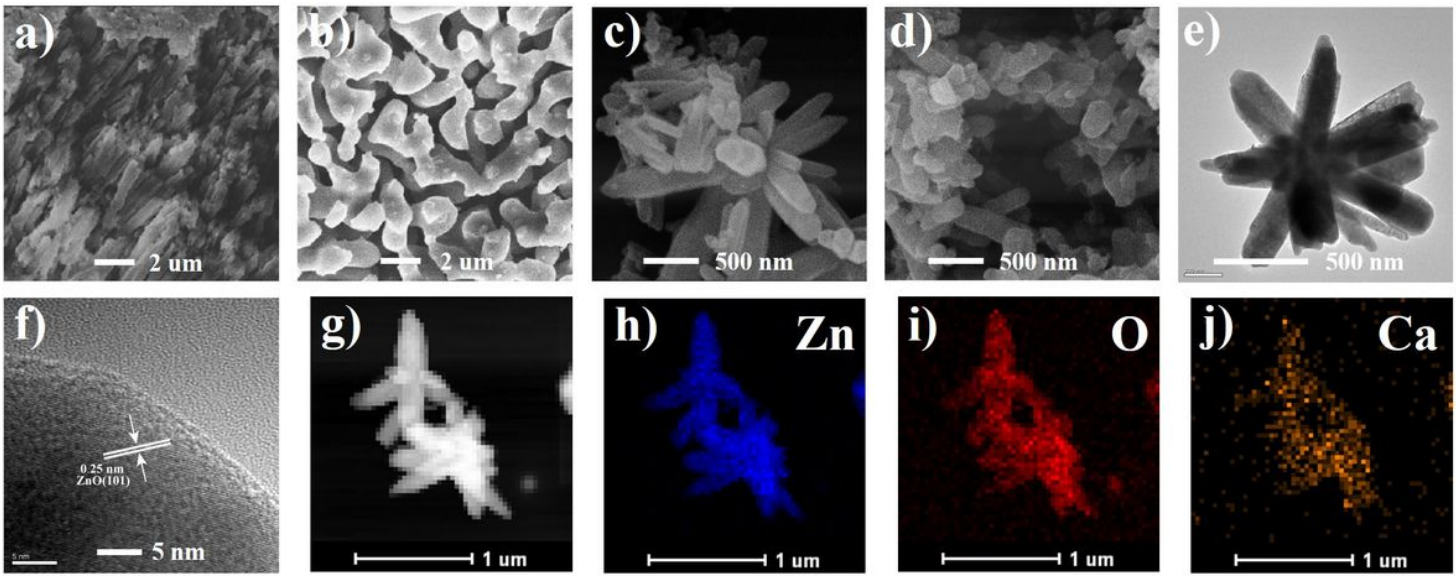

Figure 2

SEM images of snail shell (a), shell CaO (b), CaO/ZnO (c) and ZnO (d); TEM (e) and HRTEM (f) images of CaO/ZnO; EDX mapping images of CaO/ZnO (g-j)

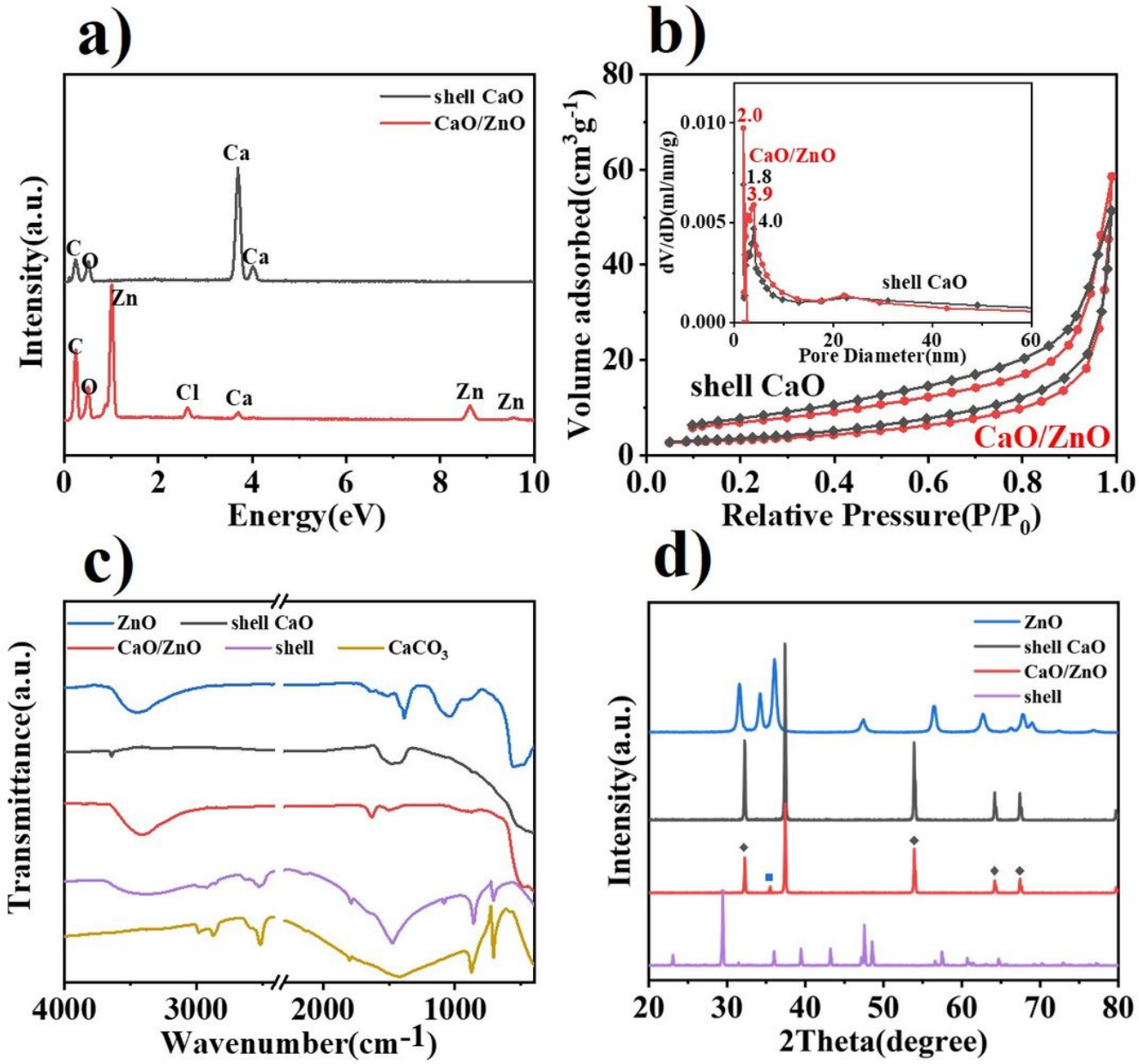

Figure 3

EDX spectra (a), N2 adsorption-desorption isotherms (b) (inset is the pore size distribution image), FT-IR spectra (c) and XRD patterns (d) of as-prepared samples

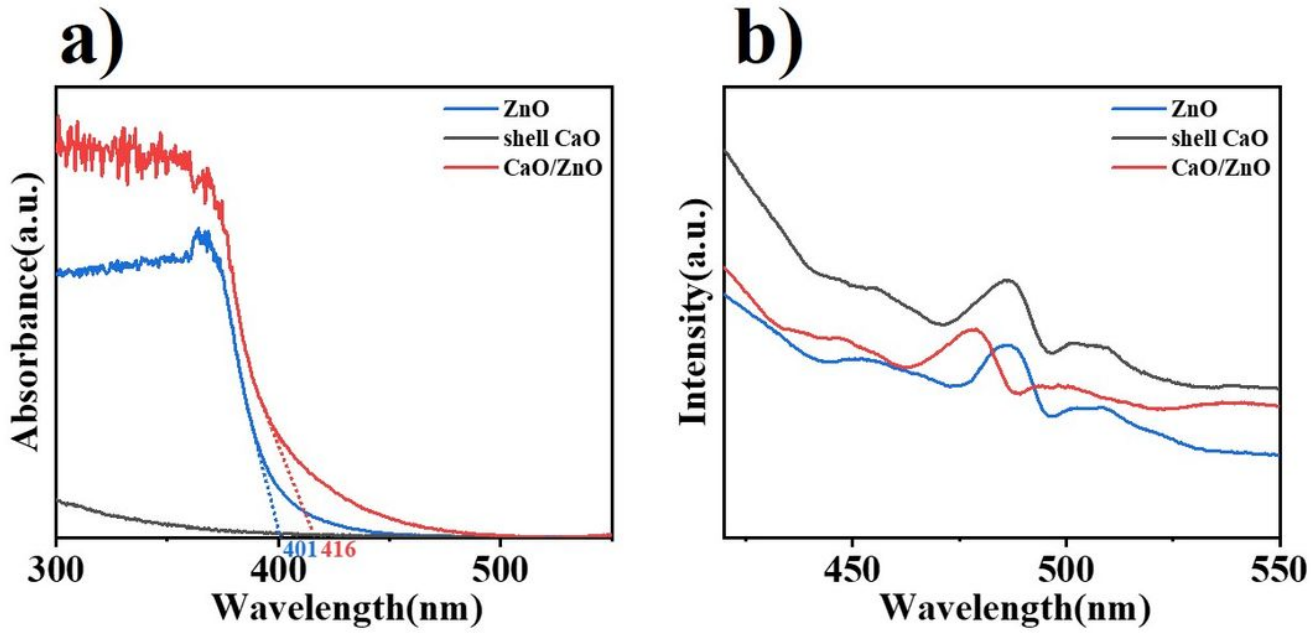

Figure 4

Diffuse reflectance UV–Vis adsorption spectra (a) and PL spectra (b) of ZnO, shell CaO and CaO/ZnO

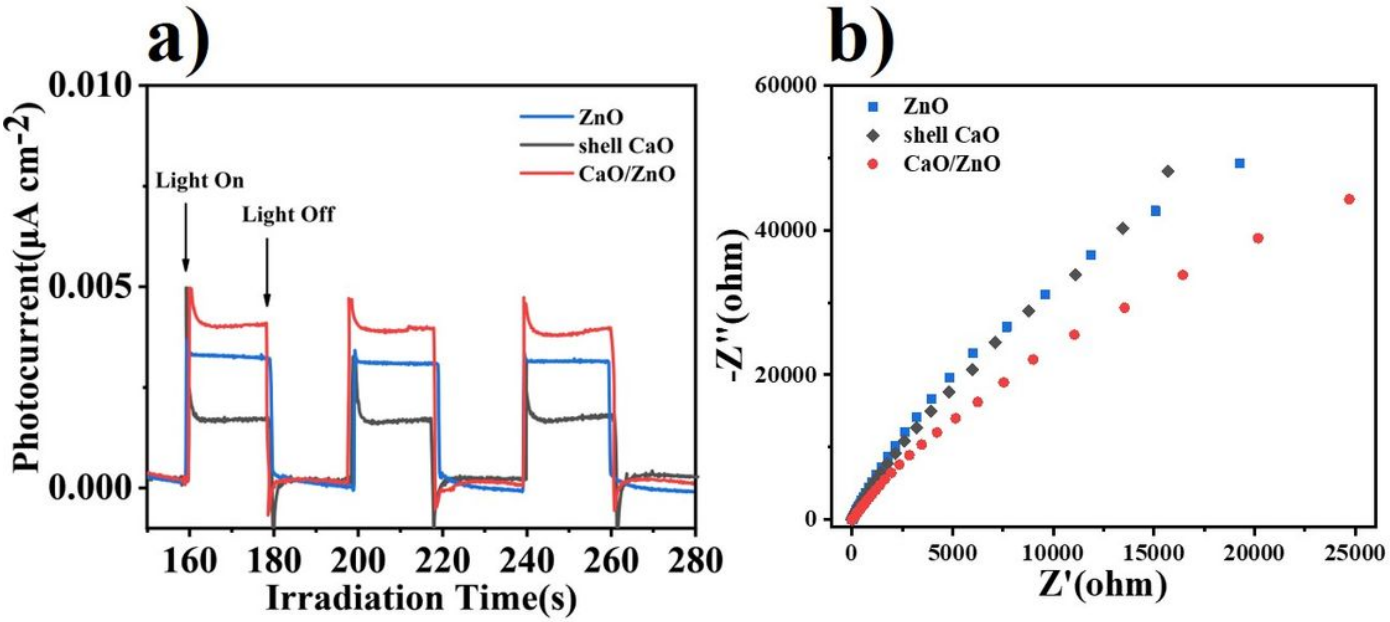

Figure 5

Photocurrent intensity (a) and Electrochemical impedance spectra (b) of ZnO, shell CaO and CaO/ZnO

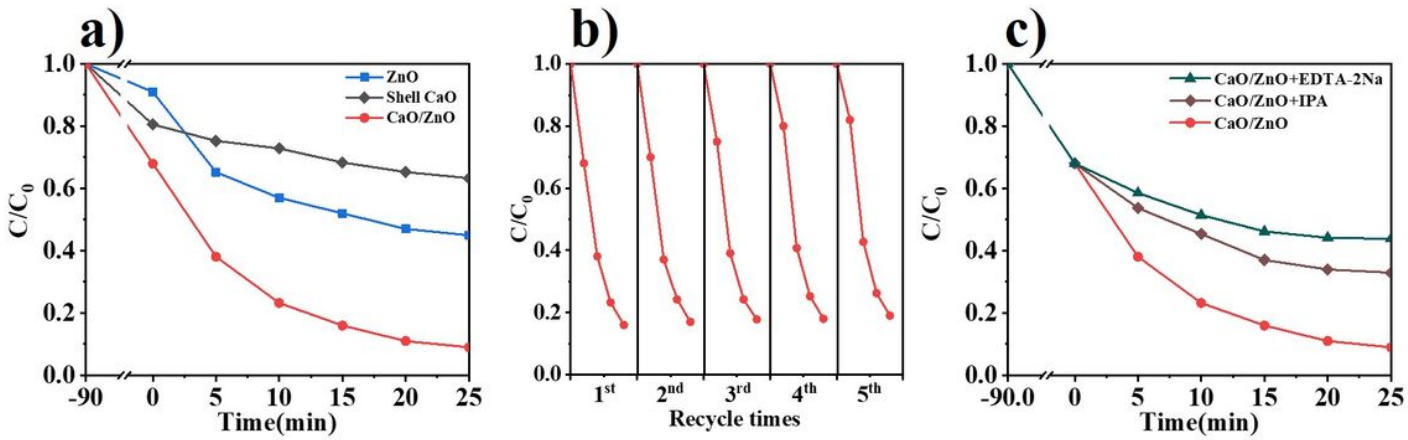

Figure 6

Removal efficiencies (a) of RhB by ZnO, shell CaO and CaO/ZnO under visible-light irradiation; degradation behaviour (b) of RhB with 5 repeated cycling of CaO/ZnO; capture experiment of active species (c) of CaO/ZnO